Technical Note: an implementation of the dry removal processes DRY DEPosition and SEDImentation in the Modular Earth Submodel System (MESSy)

A. Kerkweg, J. Buchholz, L. Ganzeveld, A. Pozzer, H. Tost, P. Jöckel

Atmos. Chem. Phys. Discuss., 6, 6853–6901, 2006
www.atmos-chem-phys-discuss.net/6/6853/2006/

Atmospheric Chemistry and Physics Discussions

Technical Note: an implementation of the dry removal processes DRY DEPosition and SEDImentation in the Modular Earth Submodel System (MESSy)

A. Kerkweg, J. Buchholz, L. Ganzeveld, A. Pozzer, H. Tost, and P. Jöckel

Air Chemistry Department, Max-Planck Institute of Chemistry, P.O. Box 3060, 55020 Mainz, Germany

Received: 8 June 2006 – Accepted: 30 June 2006 – Published: 24 July 2006

Correspondence to: A. Kerkweg (akerkweg@mpch-mainz.mpg.de)

Abstract

We present the submodels DRYDEP and SEDI for the Modular Earth Submodel System (MESSy). Gas phase and aerosol dry deposition are calculated within DRYDEP, whereas SEDI deals with aerosol particle sedimentation. Dry deposition velocities depend on the near-surface turbulence and the physical and chemical properties of the surface cover (e.g. the roughness length, soil pH or leaf stomatal exchange). The dry deposition algorithm used in DRYDEP is based on the big leaf approach and is described in detail within this Technical Note. The sedimentation submodel SEDI contains two sedimentation schemes: a simple upwind zeroth order scheme and a first order approach.

1 Introduction

The current knowledge about the dry deposition process is relatively poor (Wesely and Hicks, 2000), as dry deposition has only been measured for a relative small set of species (e.g., O_3, NO_x, HNO_3, SO_2 and sulphate) and that mostly in rather short intensive field campaigns. In addition, identification and quantification of the role of the various controlling biological, chemical and physical processes poses large challenges to the experimentalists. Consequently, a commonly applied approach to estimate the dry deposition velocities (needed to calculate the dry deposition flux) is that proposed by Wesely (1989): The solubility and reactivity of a tracer is used to estimate its dry deposition velocity relative to those of ozone and sulfur dioxide which dry deposition velocities are relatively well known. Our algorithm is adopted from prior work of Ganzeveld and Lelieveld (1995) and Ganzeveld et al. (1998). The latter already included particle sulfate dry deposition based on a predefined particle distribution. This was expanded to deal with aerosol dry deposition for online calculated aerosol distributions (Ganzeveld et al., 2006). This approach was used for the first time by Ganzeveld et al. (2006). Often, publications illustrate only the idea of an approach for the im-

ACPD

6, 6853–6901, 2006

plementation of a distinct process, but crucial details of the technical realization are omitted. This Technical Note wants to clarify the details for the MESSy submodels DRYDEP and SEDI for the sake of reproducibility. Every mathematical relationship required for the implementation is given in this article to set the reader into the position to understand and modify the code, if needed. Section 2.1.1 describes the dry deposition algorithm for trace gases, whereas Sect. 2.1.2 contains details about the aerosol dry deposition scheme. The sedimentation process is often treated together with dry deposition. But two major differences between these two processes render it useful to simulate them separately.

1. Dry deposition is only applied in the lowermost model layer, whereas sedimentation takes place within the whole vertical domain.

2. Sedimentation is a significant sink process for aerosol particles (as these carry enough mass), whereas sedimentation of trace gases is negligible.

The MESSy coding standard presents an additional reason for the separation of these two processes (Jöckel et al., 2005), as it implies the idea that every specific process is coded as a separate, independent entity, i.e. as a submodel which can be switched on/off individually.

The calculation of the sedimentation velocities is based on an approach usually found in textbooks (see Sect. 2.2). The Subsects. 2.2.1 and 2.2.2 describe the zeroth order and first order scheme, respectively. Section 2.3 focuses on the implementation of the two submodels into the MESSy system and Sect. 3 shows some examples.

2 Submodel description

DRYDEP and SEDI are implemented as independent submodels in adherence to the MESSy standard as described by Jöckel et al. (2005). This also implies a good portability due to the coding in standard Fortran95 (ISO/IEC-1539-1). No compiler-specific

language extensions are used. The code quality has been further checked by application of the Fortran analyser forcheck (http://www.forcheck.nl/).

Applying the dry deposition and/or sedimentation process to additional tracers does not require any recoding, only the definition of the Henry's law coefficient and a reactivity factor is necessary.

In the following the units of the variables in each equation within this Technical Note are explicitly given, even if the physical correctness of the equation is not dependent on the unit. This is because this Technical Note gives an overview of the implementation of the dry deposition and the sedimentation process within the MESSy submodels DRYDEP and SEDI and thus the equations as implemented in these submodels (including unit conversions) are given.

2.1 DRY DEPosition (DRYDEP)

The representation of the dry deposition process is based on the algorithm used for online calculation of dry deposition velocities according to the big leaf approach in ECHAM3 and ECHAM4 (http://www.mpimet.mpg.de/en/wissenschaft/ueberblick/atmosphaere-im-erdsystem/globale-klimamodellierung/echam.html) as published by Ganzeveld and Lelieveld (1995) and Ganzeveld et al. (1998).

2.1.1 DRY DEPosition of trace gases

The dry deposition flux $F_{\text{dep}}(X)$ (kg/(m^{2}s)) is given by

$$F_{\text{dep}}(X) = \mu_g(X) \times \frac{M(X)}{M_{\text{air}}} \times \frac{\Delta p}{g\ \Delta z} \times v_d(X) \qquad (1)$$

with $\mu_g(X)$ being the gas phase mixing ratio of species X in mol/mol and $M(X)$ and M_{air} the molar mass of species X and dry air (in kg/mol), respectively. g is the gravitational acceleration (m s^{-2}), Δp and Δz are the layer thicknesses in Pa and m, respectively.

The dry deposition velocity $v_d(X)$ of a trace gas X (in m/s) depends on the aerodynamic resistance R_a, the quasi-laminary boundary layer resistance $R_{\mathrm{qbr}}(X)$, and the surface resistance $R_s(X)$ (all resistances are in units of $\mathrm{s\,m^{-1}}$):

$$v_d(X) = \frac{1}{R_a + R_{\mathrm{qbr}}(X) + R_s(X)} \quad , \tag{2}$$

where R_a is a function of the physical state of the atmosphere, $R_{\mathrm{qbr}}(X)$ is controlled by molecular diffusion and $R_s(X)$ depends on the chemical, physical and biological properties of the surface. The resistances are given as follows:

1. The aerodynamic resistance R_a:

$$R_{a,t} = \frac{1}{u_{\star,t}\,\kappa}\left[\log\left(\frac{z}{z_{0,m}}\right) - \Phi_{h,t}\right] \tag{3}$$

with $u_{\star,t}$ being the friction velocity, κ=0.4 being the dimensionless von Karman constant, z the reference height, and $z_{0,m}$ the momentum roughness length (both in m). The dimensionless stability function $\Phi_{h,t}$ depends on the Monin-Obukhov-Length, and thus on the horizontal wind speed and the temperature profile.

In this algorithm four different surface types (t) are distinguished:

- *veg* for vegetation
- *slsn* for bare soil/snow
- *ice* for sea ice/snow and
- *wat* for water.

2. The quasi-laminar boundary layer resistance R_{qbr}:

$$R_{\mathrm{qbr},t}(X) = \ln\left(\frac{z_{0,m}}{z_{0,X}}\right)\frac{1}{u_{\star,t}\,\kappa}\left(\frac{Sc}{Pr}\right)^{2/3} \quad , \tag{4}$$

where $z_{0,m}$ and $z_{0,X}$ are the surface roughness lengths (in m) of momentum and of a trace gas X, respectively, Pr is the Prandtl number (here assumed to be 0.72), and Sc the Schmidt number, which is defined as the ratio of kinematic viscosity of air to the molecular diffusivity of a trace gas. Usually the influence of $R_{\mathrm{qbr}}(X)$ is small compared to R_a and $R_s(X)$.

3. The surface resistance $R_s(X)$:
$R_s(X)$ depends on the surface type and on the properties of the respective trace gas. In DRYDEP the calculation of the surface resistance for all the gases that are not explicitly considered in the Ganzeveld and Lelieveld (1995) and Ganzeveld et al. (1998) studies follows the approach of Wesely (1989). As the dry deposition velocities of ozone and sulfur dioxide are relatively well known, the approach of Wesely (1989) uses these two trace gases to scale all others. O_3 and SO_2 represent reactive non-soluble and non-reactive soluble trace gases, respectively. The effective Henry's law coefficient H (in mol/(dm^3 atm)) is used as a measure for the solubility of a trace gas, whereas the reactivity of a trace gas is given by a so-called reactivity coefficient s_{reac}. The empirical formulas taken from Wesely (1989) are only valid if s_{reac} has values of 1, 0.1 or 0. Here, 1 indicates a trace gas similar reactive as ozone, whereas 0 stands for a nearly non reactive gas. 0.1 is for slightly reactive gases. For more details about this approach the reader is referred to Wesely (1989). A unified formula as for R_a and R_{qbr} does not exist for the surface resistances. The individual equations are given in Appendix A2. In grid boxes over land, four different land types are taken into account:

   - the snow/ice covered fraction (index *snow*)
   - bare soil (index *soil*),
   - the water in the wet skin reservoir (index *ws*) (i.e., the fraction of the vegetation and bare soil wetted due to rain fall interception and dew fall) and
   - vegetation (index *veg*).

(Note: The types *soil* and *snow* are only distinguished for the surface resistances. For the aerodynamic resistances and the quasi-laminar boundary layer resistances these two types are combined within the type *slsn*, this simplification is justified with the assumption of comparable roughness for bare soil and snow covered surfaces.)

Over the ocean, a distinction is made between the open ocean (index *wat*) and the sea ice covered fraction which surface resistance is equal to the surface resistance for snow covered regions over land ($R_{s,snow}$).

The formulas for the calculation of the aerodynamic resistances and the surface resistances are given in Appendix A1 and A2, respectively.

As the different surface properties influence the dry deposition velocities, the actual dry deposition velocity in each grid box is a composition of the individual dry deposition velocities for the different surface types existent in the grid box. Furthermore a general classification of a box as water or land box is applied:

$$v_d(X) = \begin{cases} v_{d,\text{land}} & \text{for} \quad f_{\text{land}} \geq 0.5 \\ v_{d,wat} & \text{for} \quad f_{\text{land}} < 0.5 \end{cases}, \tag{5}$$

where f_{land} is the land covered fraction of a grid box. The dry deposition velocities over land $v_{d,\text{land}}$ are determined following

$$\begin{aligned} &v_{d,\text{land}}(X) = \\ &f_{snow} \times (R_{a,slsn} + R_{bqr,slsn}(X) + R_{s,snow}(X))^{-1} \\ &+(1 - f_{snow}) \times (1 - f_{ws}) \times f_{veg} \\ &\times (R_{a,veg} + R_{bqr,veg}(X) + R_{s,veg}(X))^{-1} \\ &+(1 - f_{snow}) \times (1 - f_{ws}) \times (1 - f_{veg}) \\ &\times (R_{a,slsn} + R_{bqr,slsn}(X) + R_{s,soil}(X))^{-1} \\ &+(1 - f_{snow}) \times f_{ws} \\ &\times (R_{a,veg} + R_{bqr,veg}(X) + R_{s,ws}(X))^{-1}. \end{aligned} \tag{6}$$

f_{snow} is the snow fraction, f_{ws} the wet skin fraction and f_{veg} the fraction of vegetation.

The dry deposition velocity over water $v_{d,wat}$ is determined by

$$v_{d,wat}(X) = (f_{si} - f_{\text{land}} \times f_{si}) \times (R_{a,ice} + R_{\text{qbr},ice}(X) + R_{s,snow}(X))^{-1} + (1 - f_{si} + f_{\text{land}} \times f_{si}) \times (R_{a,wat} + R_{\text{qbr},wat}(X) + R_{s,wat}(X))^{-1} . \quad (7)$$

f_{si} is the sea ice fraction and f_{land} is the land fraction. For the calculations of all the required resistances see Appendix A.

2.1.2 Dry deposition of aerosols

The aerosol dry deposition is also based on the big leaf approach. In contrast to the gas phase dry deposition only three surface types are distinguished:

- vegetation (index *veg*)
- bare soil and snow (index *slsn*) and
- water (index *wat*).

The overall dry deposition velocity $v_{d,p}(X)$ is determined by

$$\begin{aligned} v_{d,p}(X) &= (f_{snow} + f_{bs}) \times v_{d,p,slsn}(X) \\ &+(1 - f_{snow})(1 - f_{wat})f_{veg} \times v_{d,p,veg}(X) \\ &+(1 - f_{snow})f_{ws} \times v_{d,p,veg}(X) \\ &+f_{ice} \times v_{d,p,slsn}(X) \\ &+f_{wat} \times v_{d,p,wat}(X) . \end{aligned} \quad (8)$$

Here, f_{snow}, f_{bs}, f_{wat}, f_{veg}, f_{ws} and f_{ice} are the surface fractions of snow, bare soil, water, vegetation, wet skin and ice, respectively. The individual dry deposition velocities

(in m/s) are calculated as follows:

$$v_{d,p,veg}(X) = \left(\frac{R_{a,veg}}{100} + \frac{1}{v_{kd,p,veg}(X)} \right)^{-1} \tag{9}$$

$$v_{d,p,slsn}(X) = \left(\frac{R_{a,slsn}}{100} + \frac{1}{v_{kd,p,slsn}(X)} \right)^{-1} \tag{10}$$

$$v_{d,p,wat}(X) = \left(\frac{R_{a,wat}}{100} + \frac{1}{v_{kd,p,wat}(X)} \right)^{-1} . \tag{11}$$

The aerodynamic resistances are the same as in the gas phase dry deposition scheme (see Appendix A1). Appendix B contains the equations for the calculation of the specific dry deposition velocities $v_{kd,p,veg}$, $v_{kd,p,slsn}$ and $v_{kd,p,wat}$. They depend on the particle radius r_p, the particle density ρ_p and – for modal distributions — on the standard deviation σ_p of the mode (see also Ganzeveld et al., 2006).

For the dry deposition velocity calculation for particle mixing ratios (mol^{-1}) the ambient number median radius $r_{p,a}$ as provided by the aerosol models is taken directly, whereas for the dry deposition of aerosol compounds (e.g. SO_4^{2-}, Na^+ or Cl^-) the mass mean radius $r_{p,mm}$ is used:

$$r_p(k) = \begin{cases} r_{p,a}(k) & \text{for bins and numbers} \\ r_{p,a}(k)\, e^{3.5*(\ln \sigma_p(k))^2} & \text{for compounds of modes} \end{cases}$$

The aerosol compound dry deposition flux $F_{\mathrm{dep},c}$ in units of kg/(m^2 s) is calculated by

$$F_{\mathrm{dep},c}(X) = \mu_p(X) \times \frac{M(X)}{M_{\mathrm{air}}} \times \frac{\Delta p}{g\ \Delta z} \times v_{d,p}(X) , \tag{12}$$

where μ_p is the mixing ratio of an aerosol compound in mol/mol and $M(X)$ the molar mass of the aerosol compound (e.g. 0.096 kg/mol for SO_4^{2-}). g is the gravitational

acceleration ($m\,s^{-2}$), Δp and Δz the layer thicknesses in Pa and m, respectively.

The particle number dry deposition $F_{dep,p}$ (in $\frac{particle}{mol}\frac{kg}{m^2\,s}$) of aerosol bin/mode k is given by

$$F_{dep,p}(X) = \mu_p(X) \times \frac{\Delta p}{g\ \Delta z} \times v_{d,p}(X)\ . \tag{13}$$

$\mu_p(X)$ is here the number mixing ratio in mol^{-1}.

2.2 Aerosol SEDImentation (SEDI)

In contrast to dry deposition, which occurs in the lowermost part of the atmosphere only, sedimentation happens throughout the atmosphere. It describes the settling process due to gravity, thus it is negligible for gases, but it is an important sink for particles.

The formulas applied for the calculation of the terminal sedimentation velocity are based on the theory of aerosol sedimentation (see for example Pruppacher and Klett (1997), page 451). The terminal sedimentation velocity v_t (in m/s) is given by the Stokes velocity v_{Stokes} modified by the Cunningham-slip-flow correction f_{Csf} and the Slinn factor f_{Slinn}:

$$v_t = v_{Stokes} \times f_{Slinn} \times f_{Csf} \tag{14}$$

with

$$v_{Stokes} = \frac{2}{9}\,(\rho_p(k) - \rho_{air})\,\frac{g}{\eta_d}\,r_p(k)^2 \tag{15}$$

$$f_{Csf} = 1 + 1.257\,\frac{\lambda_{air}}{r_p(k)} + 0.4\,\frac{\lambda_{air}}{r(k)}\,exp\left(\frac{-1.1\,r_p(k)}{\lambda_{air}}\right) \tag{16}$$

$$f_{\text{Slinn}} = \begin{cases} 1 & \text{for bins and numbers} \\ \sigma_p(k)^{2/ln\sigma_p(k)} & \text{for lognormal modes} \end{cases}, \quad (17)$$

where k denotes the respective aerosol mode or bin, $\sigma_p(k)$ is the radius standard deviation, $\rho_p(k)$ the aerosol density (in kg/m^3) and $r_p(k)$ the ambient radius (in m) of aerosol mode k. η_d denotes the dynamic viscosity of air (in kg/(m^{2}s)), g the gravitational acceleration (in m/s^2) and λ_{air} the mean free path of air molecules (in m). v_{Stokes} is the sedimentation velocity of spheres in m/s. The Cunningham-slip-flow factor corrects for aerodynamic differences between ideal spheres and real non-spherical particles. In case of lognormal distributions the particle radius varies over a wide range. As the mean sedimentation velocity of all particles of a lognormal mode is larger than the sedimentation velocity for a particle of the mean radius, a correction factor has to be applied. This is the meaning of the Slinn factor f_{Slinn} (Slinn and Slinn, 1980).

There are different possibilities to calculate the change in the tracer concentration due to sedimentation with one terminal velocity. SEDI comprises two schemes: a zeroth order scheme and a first order scheme.

2.2.1 Sedimentation scheme of zeroth order/Simple upwind scheme

The sedimentation scheme of zeroth order is a simple upwind scheme. The assumption is made that all particles of one grid box are equally distributed with height. The fraction $\xi(i)$ (in 1/s) of particles falling out of one box i per time step Δt is simply determined by the geometric vertical extension of the grid box $\Delta z(i)$ (in m) and the terminal velocity v_t (in m/s):

$$\xi(i) = v_t \frac{\Delta t}{\Delta z(i)} . \quad (18)$$

In the sedimentation scheme of zeroth order the amount of particles falling down from one box into the next box below can also be associated with a cuboid moved from the lowest part of the higher box to the highest part of the box below. s_{sed} in Fig. 1

(which shows a cross section of a column of boxes) is the height of this moving cuboid. Multiplication by the mixing ratio μ_p of these particles in the respective box leads to a tracer tendency due to sedimentation out of this box:

$$\left.\frac{\Delta\mu_p(i)}{\Delta t}\right|_{\text{out}} = \xi(i) \times \frac{\mu_p(i)}{\Delta t} \tag{19}$$

Particles leaving one box enter the box below, i.e. the incoming flux F_{in} for box i equals the outgoing flux F_{out} of the box above $(i-1)$:

$$F_{\text{in}}(i) = F_{\text{out}}(i-1) = \left.\frac{\Delta\mu_p(i-1)}{\Delta t}\right|_{\text{out}} \times \frac{\Delta p(i-1)}{g} \tag{20}$$

$\Delta p(i)$ is the thickness of the box in pressure units (Pa) and g the gravitational acceleration (m/s^2). The incoming flux for the uppermost box is zero.

The tracer tendency for the lower box can be calculated using the incoming flux:

$$\left.\frac{\Delta\mu_p(i)}{\Delta t}\right|_{\text{in}} = F_{\text{in}}(i) \times \frac{g}{\Delta p(i)} \tag{21}$$

Combining Eq. (19) and Eq. (21) results in the overall tracer tendency in box i

$$\frac{\Delta\mu_p(i)}{\Delta t} = \left.\frac{\Delta\mu_p(i)}{\Delta t}\right|_{\text{in}} - \left.\frac{\Delta\mu_p(i)}{\Delta t}\right|_{\text{out}} = \left.\frac{\Delta\mu_p(i-1)}{\Delta t}\right|_{\text{out}} \times \frac{\Delta p(i-1)}{\Delta p(i)} - \left.\frac{\Delta\mu_p(i)}{\Delta t}\right|_{\text{out}} \tag{22}$$

2.2.2 Sedimentation scheme of first order/Trapezoid scheme

A possible improvement of the zeroth order sedimentation scheme described in Sect. 2.2.1 is the use of first order polynomials for the vertical profile of the mixing ratio (μ_p). The sedimentation scheme was developed in the context of the MESSy submodel PSC (a submodel for the simulation of polar stratospheric clouds, see Buchholz, 2005). With the first order scheme, the determination of the changes in the μ_p

profile due to sedimentation is no longer based on the μ_p step function shown in Fig. 1. Instead, the amount of the particle substance to move from grid box i downwards into the grid box $i+1$ is calculated by means of a straight line approximation for the μ_p profile in grid box i. The advantage of a first order vertical profile compared to the step function used in the simple upwind scheme becomes apparent by considering a local maximum in the vertical profile. Imagine a peak located around box i (see Fig. 2). A step function does not distinguish between those parts of the box $i-1$ or $i+1$ which are near the local maximum and those parts away from it. Straight line approximations for μ_p inside the grid boxes, on the contrary, can reproduce the feature that in the box above ($i-1$) more aerosol particles are located at the bottom of the box than at the top. Similarly, in box $i+1$, straight line approximations increase μ_p near the top, i.e. near the peak. Consequently, in the first order scheme more particles move from the grid box immediately above the local maximum into the next lower grid box than in the zeroth order simple upwind scheme (see Fig. 1).

The base of the first order scheme are the local straight line approximations for the mixing ratio. A straight line in the (p,μ_p)-plane is defined by the two points $(p(z_1), \mu_p(z_1))$ and $(p(z_2), \mu_p(z_2))$, where z_1 and z_2 indicate the box indices which may be i and $i+1$ or $i-1$ and i. Its slope is

$$m_{1,2} = \frac{\mu_p(z_2) - \mu_p(z_1)}{p(z_2) - p(z_1)} \tag{23}$$

and its intercept is

$$b_{1,2} = \mu_p(z_1) - \frac{\mu_p(z_2) - \mu_p(z_1)}{p(z_2) - p(z_1)}\, p(z_1) \,. \tag{24}$$

The linearly approximated mixing ratio is therefore

$$\mu_p(z) = \frac{\mu_p(z_2) - \mu_p(z_1)}{p(z_2) - p(z_1)}\, p(z)$$

ACPD
6, 6853–6901, 2006

$$+ \mu_p(z_1) - \frac{\mu_p(z_2) - \mu_p(z_1)}{p(z_2) - p(z_1)}\, p(z_1). \tag{25}$$

For the simple upwind scheme, the part of box i from which particles move into the next lower grid box $i+1$ within one model time step corresponds to a rectangle in the (p,μ_p)-plane. Using the straight line approximation for $\mu_p(z)$, this rectangle is replaced by a trapezoid (see Figs. 3 and 4).

In mathematical terms, the rectangle in the simple upwind scheme is represented by the product $\mu_p(i-1)\ s_{\text{sed}}(i-1)$.

The area of the corresponding trapezoid in the first order scheme is

$$\begin{aligned} A_{\text{trap}} &= \frac{1}{2}(\mu_p(z_1) + \mu_p(z_2))\ \Delta p_{\text{sed}}(i-1) \\ &= (m_{1,2}\ p(z_1) + b_{1,2} + m_{1,2}\ p(z_2) + b_{1,2}) \\ &\qquad \times \frac{1}{2} \times \Delta p_{\text{sed}}(i-1) \\ &= \left(m_{1,2}\ \frac{p(z_1) + p(z_2)}{2} + b_{1,2} \right) \\ &\qquad \times \Delta p_{\text{sed}}(i-1)\ . \end{aligned} \tag{26}$$

The mixing ratios $\mu_p(z_1)$ and $\mu_p(z_2)$ form the two parallel sides of the trapezoid. $\Delta p_{\text{sed}}(i-1)$ is the height of the trapezoid, which equals the distance in Pa the aerosol particles fall within one time step. (Please note: in contrast to the simple upwind scheme which works with height coordinates (in m), the first order scheme is formulated for pressure units.) As pointed out above, there are two possibilities for choosing the two points which define the straight line approximation. In addition to the box of interest (i) the grid box above ($i-1$) or the box below ($i+1$) can be chosen. There is no optimal choice in general, as each variant of the straight line approximations has advantages for some profiles and disadvantages for others. The one selected for the MESSy submodel SEDI has performed well in a series of tests within the submodels PSC (for more details see Buchholz, 2005). It is characterised by a rather

straightforward implementation as explained in the following:

Approximation above a local maximum:
If the grid box i, from which sedimentation is to be calculated, is located above a peak, the straight line is drawn through the mixing ratio values in the grid boxes i and $i+1$ (see Fig. 3). This leads to increased sedimentation compared to the simple upwind scheme.

For steep μ_p gradients above a local maximum, the above equations can lead to trapezoid areas larger than the product $\mu_p(i) \times (p_{bot}(i) - p_{top}(i))$. If these large trapezoid values are used in the sedimentation calculation, more particle substance than currently present in grid box i would be moved into grid box $i+1$. To avoid this unphysical behaviour, the transported substance is limited to the total available amount.

Approximation below a local maximum:
For grid boxes below a peak in the μ_p profile, the routine calculates the two alternative straight line approximations. The sedimentation is then calculated using the smaller trapezoid. Compared to the simple upwind scheme, sedimentation below a local maximum is reduced (see Fig. 4).

The above choice leads to the use of μ_p values from the grid box i and $i-1$, if $\mu_p(i)$ is relatively small compared to $\mu_p(i-1)$ (see left hand side of Fig. 5). These cases are interpreted as a local maximum in the vertical μ_p profile which is mainly in grid box $i-1$, but extends slightly into grid box i. Thus it seems appropriate to approximate $\mu_p(i-1)$ in such a way that most particles are located in the upper part of grid box i. For steep μ_p gradients, however, the above equations can lead to negative trapezoid areas. In those cases, no particle sedimentation takes place.

For $\mu_p(i)$ values only slightly below $\mu_p(i-1)$, the vertical μ_p profile is interpreted as a peak which has fully arrived in grid box i and extends into grid box $i+1$. The vertical μ_p profile near the i to $(i+1)$ interface is thus best approximated by means of $\mu_p(i)$ and $\mu_p(i+1)$ (see Fig. 5).

ACPD
6, 6853–6901, 2006

EGU

Treatment of local extrema:
For local extrema in the vertical μ_p profile, the influence of nearby grid boxes on the particle distribution inside grid box i is less evident. Therefore, if the grid box i under consideration is a local maximum or a local minimum, the vertical μ_p profile is not approximated by straight lines. Hence the area which defines the amount of sedimenting substance is not a trapezoid but a rectangle corresponding to the product $\mu_p(i)\Delta p_{\text{sed}}(i-1)$, similar to the simple upwind scheme.

Finally, it is important to note that in both schemes are not monotonic as it is necessary for sedimentation schemes, as a particle mixture can disperse, because larger particles fall faster than smaller ones. This characteristic in particular rules out the application of advection algorithms for simulating the process of sedimentation, since advection requires monotonicity (Buchholz, 2005).

2.3 Integration of the submodels into the MESSy system

The key component to automatise the calculation for all tracers is the functionality provided by the generic MESSy submodel TRACER. The properties of the tracers including the switches which processes should be applied to the tracers are all stored within the meta-information structure provided by the submodel TRACER and are defined during the definition of a tracer (see Jöckel et al., 2006[1]).

2.3.1 Gas phase dry deposition

The important information held by the tracer meta-information structure required for the gas phase tracer dry deposition are:

– `medium`: The medium of the tracer must be `AIR`

[1] Jöckel, P., in preparation, 2006.

– `ndrydep`: This switch must be set to `ON` indicating that a tracer should be subject to dry deposition.

– `molarmass` and `henry`: with exception of H_2SO_4 the molar mass and the Henry's law coefficient (in mol/(dm^3 atm)) must be declared when the tracer is defined, if the tracer should be deposited within DRYDEP.

– `dryreac_sf`: This is the factor especially defined for dry deposition calculations. `dryreac_sf` is the factor s_{reac} (see Sect. 2.1.1 and Appendix A2). It scales the reactivity of a respective tracer to the reactivities of ozone and sulfur dioxide.

If a tracer fulfils all these requirements the dry deposition velocity for this tracer is calculated according to the formulas given in Sect. 2.1.1 and in Appendix A.

To take into account that the concentration used to calculate the dry deposition flux continuously decreases during the time step due to dry deposition and to avoid total depletion in one grid box for very efficiently depositing species (e.g. HNO_3) the effective dry deposition velocity $v_{d,\text{eff}}$ (in m/s) is calculated from the dry deposition velocity v_d (calculated as described in Sect. 2.1), according to

$$v_{d,\text{eff}} = \frac{\Delta z}{\Delta t} \times \left[1 - \exp\left(-v_d \frac{\Delta t}{\Delta z}\right)\right] \tag{27}$$

with Δt time step in s and Δz layer thickness in m.

From this effective dry deposition velocity and the current tracer mixing ratio μ (in mol/mol) the dry deposition flux F_{ddep} (in $\frac{\text{mol}}{\text{mol}} \frac{\text{kg}}{(\text{m}^2\,\text{s})}$) is calculated by

$$F_{\text{ddep}} = \mu \times \frac{\Delta p}{g \Delta z} \times v_{d,\text{eff}} \tag{28}$$

DRYDEP provides two possibilities to assign the dry deposition flux to the tracer.

– The flux is directly provided as the lower boundary condition for the vertical diffusive flux.

– A tracer tendency $\left(\Delta\mu/\Delta t \text{ in mol}/(\text{mol s})\right)$ is calculated from the flux:

$$\frac{\Delta\mu}{\Delta t} = F_{\text{ddep}} \times \frac{\Delta p}{g} \tag{29}$$

This tendency is then applied to the tracer within the time integration scheme of the base model.

In the diagnostic output, the dry deposition flux $F_{\text{ddep,diag}}$ in the more common units of $\text{m}^{-2}\,\text{s}$ is given, calculated by

$$F_{\text{ddep,diag}} = F_{\text{ddep}} \times \frac{N_A}{10^{-3} M_{\text{air}}} \tag{30}$$

with N_A Avogadro constant ($6.022\times10^{23}\,\text{mol}^{-1}$) and M_{air} the molar mass of dry air in g/mol.

2.3.2 Aerosol dry deposition and sedimentation

The processing of aerosol tracers subject to dry deposition and/or sedimentation is very similar. Both submodels take advantage of the TRACER meta-information structure. During the initialization phase of the submodels all tracers are tested if their flags `ndrydep` or `nsedi` for dry deposition or sedimentation, respectively are switched `ON`, and if the `medium` of the tracer is `AEROSOL`. In this case the name of the aerosol model (with which the tracer is associated) is memorised[2]. Thereafter, it is checked whether the required aerosol models are running. For all tracers which are associated with an aerosol model that is not switched on, no dry removal (neither dry deposition,

[2]The automatic detection of the required aerosol models by inquiring the TRACER meta-information structure is not part of the versions of the DRYDEP and SEDI code included in version 1.1 of MESSy, but will be provided with future releases. In version 1.1 instead, a list of all aerosol models implemented in MESSy is coded.

nor sedimentation) is calculated. This is because the dry removal of an aerosol particle depends on its properties, i.e. on the radius r_p (in m), the aerosol density ρ_p (in kg m^{-3}) and – for modal distributions – on the standard deviation σ_p (see Appendix B and Sect. 2.2.1 for DRYDEP and SEDI, respectively.) These three input fields for each aerosol model are obtained via the MESSy data transfer/export interface. This also includes the information about the number of modes and/or bins treated in the respective aerosol model.

The terminal velocities are calculated for each mode/bin of each aerosol model. After those calculations are finished for all aerosol models, each tracer is checked for its `medium` and the flags `ndrydep` or `nsedi`. For the flux calculation of the individual tracer, the terminal velocity of the mode/bin of the corresponding aerosol model is used.

In addition to the three dimensional application, simple box models exist which calculate in dependence on the aerosol radius, the aerosol density and the standard deviation the aerosol dry deposition or aerosol sedimentation velocities, respectively. Results of these box models are shown in Sect. 3.2.

2.3.3 Coupling to the AIRSEA submodel

The MESSy submodel AIRSEA (Pozzer et al., 2006[3]) determines the exchange of distinct tracers at the ocean surface. These exchanges are net fluxes of emission and dry deposition. Thus it is desirable to switch off the dry deposition calculation of the respective tracer in grid boxes over the ocean, to avoid "double counting" of this removal process. DRYDEP automatically tests if the submodel AIRSEA is switched on, and which tracers are affected. For those tracers whose ocean/atmosphere exchange is calculated directly by AIRSEA, the calculated dry deposition velocity within DRYDEP

[3]Pozzer, A. and Jöckel, P. and Sander, R., Ganzeveld, L., and Lelieveld, J.: Technical Note: The MESSy-submodel AIRSEA calculating the air-sea exchange of chemical species, Atmos. Chem. Phys. Discuss., submitted, 2006.

is set to zero for grid boxes with a land fraction smaller than 0.5:

$$v_d = \begin{cases} v_d & for \quad f_{\text{land}} \geq 0.5 \\ 0 & for \quad f_{\text{land}} < 0.5 \end{cases}. \tag{31}$$

3 Examples

3.1 Gas phase dry deposition

As ozone and sulfur dioxide are the two trace gases to which the other gases are scaled, Figs. 6 and 7 depict the annually averaged dry deposition velocities of ozone and sulfur dioxide, respectively. Ozone reaches the highest deposition velocities over land due to the dense vegetation cover in summer associated with an efficient uptake by the stomata, whereas SO_2 shows its deposition maxima over the oceans, due to its higher solubility.

Figure 8 shows the annually averaged dry deposition velocity of peroxy acetyl nitrate (PAN). PAN is associated with a reactivity coefficient of s_{reac}=0.1, i.e. the reactivity of PAN is between those of ozone and sulfur dioxide. The same holds for the solubility. According to its effective Henry coefficient PAN is more soluble than ozone, but less soluble than SO_2 (see Table 1 for the assumed reactivity coefficients and the effective Henry coefficients).

The scaling of the deposition velocity of PAN between those of the two trace gases ozone and SO_2 becomes obvious in the desert regions and over the oceans. In the desert regions the deposition velocities of PAN are smaller than those of ozone showing minima similar to the SO_2 deposition velocities in these regions. Over the ocean the dry deposition velocities are smaller for PAN compared to ozone. As the effective Henry coefficient of PAN is smaller than that of SO_2 the first summand in Eq. (A15), Appendix A2 is small and the second summand dominates the resistance. As the reactivity coefficient for PAN is smaller than for ozone, the sea uptake resistance is larger for PAN resulting in a smaller dry deposition velocity compared to ozone.

Formic acid (HCOOH, see Fig. 9) is a second example for a species which dry deposition velocity is calculated by scaling to SO_2 and ozone. The reactivity coefficient is 0, as for SO_2, but the solubility of HCOOH is higher than the solubility of the two other trace gases. This causes higher dry deposition velocities as compared to SO_2 and ozone.

3.2 Aerosol dry removal: box model examples

The following two examples are calculated in simple boxmodels prescribing standard pressure (101 325 Pa) and a temperature of 298.15 K as environmental conditions.

3.2.1 Aerosol sedimentation velocities

Figure 10 illustrates the dependency of the sedimentation velocity of aerosol particles on the aerosol density and on the particle radius. The curves are shown for radii of 20 nm, 40 nm, 80 nm, 160 nm, 320 nm and 640 nm, respectively. The sedimentation velocity increases with increasing density and increasing radius.

3.2.2 Aerosol dry deposition velocities

In Fig. 11 the aerosol dry deposition velocity (in m/s) is shown versus the aerosol radius calculated for land surfaces and for three different aerosol densities. To give a range of realistic dry deposition velocities, the densities of 500 kg m^{-3}, 1500 kg m^{-3} and 3000 kg m^{-3} are chosen to cover the usual aerosol density range.

The aerosol dry deposition velocity as function of the aerosol radius shows a minimum around 0.5 μm. The influence of the aerosol density is negligible for aerosol radii below approximately 1 μm. For particles larger than 1 μm the dry deposition velocities are the higher the denser the particle is.

ACPD
6, 6853–6901, 2006

4 Summary

We have presented the new MESSy submodels DRYDEP and SEDI for dry deposition of gas and aerosol tracers and sedimentation of aerosol particles, respectively. As part of the community model MESSy they are available to our colleagues in atmospheric chemistry and climate research upon request. See http://www.messy-interface.org for details.

Appendix A

Calculation of resistances

A1 Aerodynamic resistances

The aerodynamic resistances strongly vary depending on the three surface types land, water and ice/snow. The aerodynamic resistance over land is split into a bare soil and snow (*slsn*) and a vegetation (*veg*) part. Thus, in Eq. (3) the index t indicates the surface type, i.e., t is one of *veg* (vegetation), *slsn* (bare soil/snow), *ice* (sea ice/sea snow) and *wat* (water).

Some special assumptions are made for the roughness length $z_{0,m}$ (in m). It is set to 0.005 m for the surface type *slsn* and for the surface type *veg* it is set to a minimum of 0.02 m if the prescribed roughness length $z_{0,m,\mathrm{pre}}$ is smaller than 0.02. For all other surface types the unchanged $z_{0,m,\mathrm{pre}}$ is used. The prescribed roughness length and the prescribed Leaf Area Index (LAI, used for the calculation of the surface resistance over vegetation in Eq. A7) have been preprocessed using land cover data (Olson, 1992) and additional NDVI (Normalised Difference Vegetation Index) data. For more information see Ganzeveld et al. (2002) and Ganzeveld et al. (2006).

The friction velocity $u_{\star,t}$ (m/s) depends on the surface type t:

$$u_{\star,t} = \sqrt{c_{m,t}} \times |v_h| \tag{A1}$$

where $|v_h| = \sqrt{(u^2+v^2)}$ is the horizontal wind speed (in m/s), and the dimensionless, surface type dependent drag coefficient $c_{m,t}$ is the product of the neutral drag coefficient $c_{nd,t}$, the momentum drag (md) coefficient $c_{md,t}$ and the exchange parameter $c_{ex,t}$ (all dimensionless and provided by the base model):

$$c_{m,t} = \frac{c_{nd,t} \times c_{md,t}}{c_{ex,t}} \tag{A2}$$

Note, that all these coefficients depend on the surface type.

The stability function $\Phi_{h,t}$ not only depends on the surface type, but also on the Richardson number (Ri), which is provided by the base model, (see e.g. Stull, 1988, pp.383):

- $Ri > 0$, i.e. stable conditions:
  In this case the stability function depends on the Monin-Obukhov-Length L (m), and on the layer thickness Δz in m.

$$\Phi_{h,t} = 4.7 \times \frac{\Delta z}{L} \tag{A3}$$

- $Ri \leq 0$, i.e. neutral and unstable conditions: The stability function $\Phi_{h,t}$ depends on the profile functions at the surface Ψ_h. This is constant for neutral conditions

$$\Psi_{h,\mathrm{neut}} = 0.74$$

and depends on the Richardson number for unstable conditions

$$\Psi_{h,t,us} = 0.74 \times \sqrt{1 - 9\, Ri_t} \quad . \tag{A4}$$

The constant 0.74 is an approximation for the ratio of the diffusivities of heat and momentum (see Stull, 1988, p.384 for details). The dimensionless stability function $\Phi_{h,t}$ is then given by

$$\Phi_{h,t} = \left[2\log\left(\frac{1+\Psi_{h,t,us}}{2}\right) + \log\left(\frac{1+\Psi_{h,t,us}^2}{2}\right) - 2\arctan(\Psi_{h,t,us})\right] - \left[2\log\left(\frac{1+\Psi_{h,\text{neut}}}{2}\right) + \log\left(\frac{1+\Psi_{h,\text{neut}}^2}{2}\right) - 2\arctan(\Psi_{h,\text{neut}})\right] . \quad \text{(A5)}$$

A2 Surface resistances

As stated above, the calculation of the surface resistances for most of the trace gases is taken from Wesely (1989). Thus most of the following equations can be found in that paper where also more details are given about the ideas of this parameterization. The surface resistances depend on the properties of the individual trace gas X. They are calculated according to Wesely (1989), except of the trace gases listed in Table 2. These specific surface uptake resistances are explicitly calculated according to parameterizations described in more detail below or are assigned specific values based on a extensive review of available observations (see Ganzeveld and Lelieveld, 1995; Ganzeveld et al., 1998). For most of the trace gases, the surface resistances are estimated from the respective resistances of SO_2 and O_3. The factor $s_{\text{reac}}(X)$ defines a weight, i.e., whether a species behaves more like SO_2 or O_3. In addition to SO_2 and O_3, most surface resistances of HNO_3, NO and NO_2 are also predefined and not

calculated (see Table 2). The exceptions (indicated by a letter in Table 2) are explained in detail at the end of this section.

The surface resistances required for the calculation of the dry deposition velocities in Eqs. (6) and (8) are determined as follows:

- The surface soil resistance $R_{s,soil}(X)$:
  The parameterization is given by Wesely (1989) Eq. (9).

$$R_{s,soil}(X) = \left(\frac{H(X)}{10^5 \times R_{s,soil,\mathrm{SO_2}}} + \frac{s_{\mathrm{reac}}(X)}{R_{s,soil,\mathrm{O_3}}} \right)^{-1} \tag{A6}$$

  Where $H(X)$ is the Henry's law coefficient in mol/(dm^3 atm) of the respective trace gas X. $R_{s,soil,\mathrm{SO_2}}$ and $R_{s,soil,\mathrm{O_3}}$ are the soil surface resistances of SO_2 and O_3, respectively.

- Surface vegetation resistance $R_{s,veg}(X)$:

$$R_{s,veg}(X) = \left[\left(R_{\mathrm{can}} + R_{\mathrm{qbr},veg}(X) + R_{s,soil}(X) \right)^{-1} + \left(\frac{\mathrm{LAI}}{R_{\mathrm{leaf}}(X)} \right) \right]^{-1} \tag{A7}$$

  $R_{s,soil}$ is the soil surface resistance as defined in the previous item and $R_{\mathrm{qbr},veg}$ is the quasi-laminar boundary layer resistance for vegetation, as described by Eq. (4). LAI is the prescribed leaf area index in m^{2}m^{-2}. The canopy resistance R_{can} is calculated by

$$R_{\mathrm{can}} = 14 \times \frac{h_{\mathrm{can}}}{u_{\star,veg}} \quad , \tag{A8}$$

ACPD
6, 6853–6901, 2006

where h_{can} is the canopy height (m) and $u_{\star,veg}$ the friction velocity for vegetation (m/s). The leaf resistance R_{leaf} depends on the cuticular resistance R_{cut}, the mesophyll resistance R_{mes} and on the stomatal resistance corrected for differences between water and the respective species X, $R_{stom,corr}(X)$:

$$R_{leaf}(X) = \left(\frac{1}{R_{cut}(X)} + \frac{1}{R_{stom,corr}(X) + R_{mes}(X)} \right)^{-1} . \quad \text{(A9)}$$

The three resistances are determined by

– Mesophyll resistance $R_{mes}(X)$:

$$R_{mes}(X) = \left(\frac{H(X)}{3000} + 100 \times s_{reac}(X) \right)^{-1} , \quad \text{(A10)}$$

as given by Eq. (6) in Wesely (1989).

– Cuticular resistance $R_{cut}(X)$:

$$R_{cut}(X) = \frac{R_{cut,O_3}}{10^{-5} \times H(X) + s_{reac}(X)} , \quad \text{(A11)}$$

see Eq. (7) by Wesely (1989).

– Corrected stomatal resistance $R_{stom,corr}(X)$:
The calculation of this term is based on Wesely (1989) Eq. (4):

$$R_{stom,corr}(X) = \frac{M(X)}{M_{H_2O}} \times \frac{R_{stom}}{\Psi_{sm}} . \quad \text{(A12)}$$

Here, $M(X)$ and M_{H_2O} are the molar masses of the species X and water, respectively (g mol^{-1}). R_{stom} is the leaf stomatal resistance (s m^{-1}) and Ψ_{sm} the soil moisture stress function. Both are provided by the base model.

- Surface snow resistance $R_{s,snow}(X)$:

$$R_{s,snow}(X) = \left(\frac{H(X)}{10^5 \times R_{s,snow,SO_2}} + \frac{s_{reac}(X)}{R_{s,snow,O_3}} \right)^{-1} \quad \text{(A13)}$$

This formula is given by Wesely (1989) Eq. (8).

- Wet skin resistance $R_{s,ws}(X)$:
The solubility of the trace gas is of special importance in the wet skin fraction (see Wesely (1989), Eq. 14):

$$R_{s,ws}(X) = \left(\frac{1/3}{R_{s,ws,SO_2}} + 10^{-7} \times H(X) + \frac{s_{reac}(X)}{R_{s,ws,O_3}} \right)^{-1} \quad \text{(A14)}$$

- Sea uptake resistance $R_{s,wat}(X)$:

$$R_{s,wat}\ (X) = \left(\frac{H(X)}{10^5 \times R_{s,wat,SO_2}} + \frac{s_{reac}(X)}{R_{s,wat,O_3}} \right)^{-1} \quad \text{(A15)}$$

A2.1 Special cases

Table 2 lists the predefined resistances used to calculate the surface resistances. There are three exceptions indicated by the letters A and B within the table.

A: The mesophyll resistances of NO and NO_2 are calculated from the corrected stomatal resistance of ozone:

$$R_{mes}(NO) = 5 \times R_{stom,corr,O_3} \quad \text{(A16)}$$

$$R_{mes}(NO_2) = 0.5 \times R_{stom,corr,O_3} \quad \text{(A17)}$$

B: For SO_2 and HNO_3 the surface resistances over snow are mainly determined by the surface temperature T_s

$$R_{s,snow}(SO_2) = R_{s,snow}(HNO_3) = 10.^{(-0.09*(T_s-273.)+2.4)} \quad \text{(A18)}$$

The resistances are further limited to a maximum and minimum value:

$$10 \leq R_{s,snow}(SO_2) = R_{s,snow}(HNO_3) \leq 10^5 \quad \text{(A19)}$$

C: The soil resistance of SO_2 is soil pH dependent. For the calculation of $R_{s,soil}(SO_2)$ 5 soil pH classes j (as given by Batjes, 1995) are distinguished. Each of these classes is associated with a prescribed soil resistance $R_{s,soil}(j)$. Table 3 lists the different pH classes and the respective soil resistances. The final soil resistance for SO_2 is given by

$$R_{s,soil}(SO_2) = 1000 \times \exp(269 - T_s) + \sum_j f_j \times R_{soil,j} \; . \quad \text{(A20)}$$

The f_j denote the grid-box fractions with soil pH class j.
The soil resistance is further modified for arid regions (relative humidity in 2 m above surface (rh_2) less than 0.4):

$$R_{soil,arid}(SO_2) = R_{s,soil}(SO_2) * 3.41 - 85 + ((0.4 - rh_2)/0.4) * 1.e5) + 1000 \times \exp(269 - T_s) \quad \text{(A21)}$$

and for semi-arid regions (0.4< rh_2 <0.6)

$$R_{\text{soil,semi-arid}}(SO_2) = R_{s,soil}(SO_2) * 3.41 - 85 + 1000 \times \exp(269 - T_s). \quad \text{(A22)}$$

More details about this approach to account for the soil pH dependence of the soil resistance are found in Ganzeveld et al. (1998).

Appendix B

Calculation of aerosol dry deposition velocities

- The particle dry deposition velocity over vegetation $v_{kd,p,veg}$ is given by

$$v_{kd,p,veg} = \exp(-St_{veg}^{-0.5}) \times (v_{b,veg} + v_{im,veg} + v_{in,veg}) \quad \text{(B1)}$$

The variables are

– the dimensionless Stokes number over vegetation covered surfaces St_{veg}

$$St_{veg} = f_{\text{relax}} \frac{100 \times u_{*,veg}^2}{g \times 0.1} \quad \text{(B2)}$$

where $u_{\star,veg}$ is the friction velocity as above, g is the gravitational acceleration, and 0.1 is the characteristic radius (in cm) for the so-called "largest collector" (= aerosol particle). The relaxation factor f_{relax} is given by

$$f_{\text{relax}} = 10^{-3} \frac{\rho_p (\alpha r_p)^{2\beta} \cdot f_{\text{cun}}}{18 \eta_d \kappa} \tag{B3}$$

with ρ_p aerosol density (in kg m^{-3}), r_p the particle radius (in cm), η_d dynamical viscosity $\left(=1.789\times10^{-4}\,\text{g/(cm s)}\right)$, κ=0.4 von Karman constant and α and β given as follows:

$$\begin{aligned}\alpha = {} & 1 - (10.2 - 23.7\,s + 14.5\,s^2)(1 - 0.6) \\ & - (-6.7 + 15.5\,s - 9.2\,s^2)(1 - 0.6^2) \\ & + 1.2 \exp\left(\frac{0.066 \times s}{\Phi - s}\right)\end{aligned} \tag{B4}$$

$$\beta = \exp\left(\frac{0.00077 \times s}{1.009 - s}\right) \tag{B5}$$

$$\text{with } \Phi = 1.058 - \frac{0.0155\,(s - 0.97)}{1.02 - s^{1.4}} \tag{B6}$$

where s is the relative humidity in 2 m above the surface (in %). The Cunningham-slip-flow correction factor f_{cun} is given by

$$f_{\text{cun}} = 1 + \frac{\lambda_p}{\alpha r_p^{\beta}} \left(1.257 + 0.4 \exp\left(-\frac{1.1 r_p}{\lambda_p}\right)\right) \tag{B7}$$

λ_p=0.066×10^{-4} cm is the free mean path of a particle.

– $v_{b,veg}$ is the dry deposition velocity due to Brownian diffusion:

$$v_{b,veg} = \frac{100 \times u_{\star,veg}^2}{\kappa |v_h|} Sc^{\frac{2}{3}} \tag{B8}$$

with $u_{\star,veg}$, κ and $|v_h|$ given as above. The Schmidt number Sc is calculated by

$$Sc = \frac{\nu}{D_c} = 0.15 \times \left(\frac{k_B T_s f_{\text{cun}}}{3\pi \eta_d \alpha r_p^{\beta}} \right)^{-1} \tag{B9}$$

ν is the kinematic viscosity (0.15 cm^2/s), k_B is the Boltzmann constant $\left(1.38 \times 10^{-23} (\text{J/K})\right)$, T_s (K) is the surface temperature and η_d, α, r_p and β are given as above.

– $v_{im,veg}$ is determined by the impact of the vegetation surface

$$v_{im,veg} = \frac{100 \times u_{\star,veg}^2}{\kappa |v_h|} \times \frac{St_{veg}^2}{1 + St_{veg}^2} \tag{B10}$$

– $v_{in,veg}$ is that part of the deposition including the interception collection efficiency:

$$v_{in,veg} = \frac{100 \times u_{\star,veg}^2}{\kappa |v_h|} \times \frac{1}{2} \left(\frac{r_p}{10^{-4}} \right)^2 \tag{B11}$$

- The particle dry deposition velocity for snow and bare soil $v_{kd,p,slsn}$ is calculated in a similar way:

$$v_{kd,p,slsn} = v_{b,slsn} + v_{im,slsn} \tag{B12}$$

with dry deposition due to Brownian diffusion:

$$v_{b,slsn} = \frac{100 \times u_{\star,slsn}^2}{\kappa |v_h|} Sc^{\frac{2}{3}} \tag{B13}$$

and due to impaction

$$v_{im,slsn} = \frac{100 \times u_{\star,slsn}^2}{\kappa |v_h|} \times 10^{-\frac{3}{St_{slsn}}} \quad , \tag{B14}$$

where St_{slsn} is the dimensionless Stokes number for bare soil and snow

$$St_{slsn} = f_{\text{relax}} \frac{100 \times u_{\star,slsn}^2}{\nu} \quad . \tag{B15}$$

- The dry deposition velocity over water $v_{kd,p,wat}$ is calculated following Hummelshøj et al. (1992) :

$$v_{kd,p,wat} = (1 - \alpha)(v_{b,wat} + v_{im,wat}) + \alpha v_{\text{bubble}} \tag{B16}$$

Equation (B16) is equivalent to Eq. (10) in the paper of Hummelshøj et al. (1992). α is the relative area of bursting bubbles, approximated by

$$\alpha = 1.7 \cdot 10^{-6} \times v_{10,h}^{3.75} \tag{B17}$$

(see Hummelshøj et al. (1992), Eq. 12).

$v_{b,wat}$ is the dry deposition velocity due to Brownian diffusion, given by

$$v_{b,wat} = \frac{100}{3} \times u_{\star,wat} \times Sc^{-0.5} \times Re^{-0.5} \tag{B18}$$

with Re Reynolds number and Sc Schmidt number. $v_{im,wat}$ is the impaction velocity

$$v_{im,wat} = 100 \times u_{\star,wat} \times 10^{-\frac{3}{St_{wat}}} \tag{B19}$$

St_{wat} is the dimensionless Stokes number for water

$$St_{wat} = f_{\text{relax}} \frac{100 \times u^2_{\star,wat}}{\nu} \tag{B20}$$

and v_{bubble} describes the influence of bubble bursting and consists of two parts:

$$v_{bubble} = \frac{100 \times u^2_{\star,wat}}{|v_h|} + Eff \times 2\pi r_d^2 \times 2r_h \times 500 \quad . \tag{B21}$$

The first part describes the atmospheric diffusion velocity, and the second part the wash out velocity. The collection efficiency Eff is assumed to be 0.5, $2\pi r_d^2$ is the area of a spray drop (r_d in m), and r_h is the average height reached by the spray drop (in m). For more details see Hummelshøj et al. (1992).

Acknowledgements. We thank all MESSy developers and users for their support. We have used the Ferret program (http://www.ferret.noaa.gov) from NOAA's Pacific Marine Environmental Laboratory for creating some of the graphics in this paper.

References

Batjes, N. H.: A global data set of soil pH properties, Tech. Rep. 27, Int. Soil Ref. and Inf. Cent., Wageningen, Netherlands, 1995. 6880

Buchholz, J.: Simulations of Physics and Chemistry of Polar Stratospheric Clouds with a General Circulation Model, Ph.D. thesis, Johannes Gutenberg-Universität, Fachbereich Physik, http://nbn-resolving.de/urn/resolver.pl?urn=urn:nbn:de:hebis:77-8187, 2005. 6864, 6866, 6868

Ganzeveld, L. and Lelieveld, J.: Dry deposition parameterization in a chemistry general circulation model and its influence on the distribution of reactive trace gases, J. Geophys. Res., 100, 20 999–21 012, 1995. 6854, 6856, 6858, 6876

Ganzeveld, L., Lelieveld, J., and Roelofs, G.-J.: A dry deposition parameterization for sulfur oxides in a chemistry and general circulation model, J. Geophys. Res., 103, 5679–5694, 1998. 6854, 6856, 6858, 6876, 6881

Ganzeveld, L., Lelieveld, J., Dentener, F., Krol, M., and Bouwman, A. J.: Global soil-biogenic NO_x emissions and the role of canopy processes, J. Geophys. Res., 107, 4298, doi:10.1029/2001JD001289, 2002. 6874

Ganzeveld, L., Aardenne, J., Butler, T., Lawrence, M., Metzger, S., Stier, P., Zimmermann, P., and Lelieveld, J.: Anthropogenic and natural offline emissions and the online EMission and dry DEPosition submodel EMDEP of the Modular Earth Submodel System (MESSy), Atmos. Chem. Phys. Discuss., 6, 5457–5483, 2006. 6854, 6861, 6874

Hummelshøj, P., Jensen, N., and Larson, S.: Precipitation scavenging and atmosphere-surface exchange, chap. Particle dry deposition to as sea surface, 820–840, Hemisphere Publishing Corporation, Washington, 1992. 6884, 6885

Jöckel, P., Sander, R., Kerkweg, A., Tost, H., and Lelieveld, J.: Technical Note: The Modular Earth Submodel System (MESSy) – a new approach towards Earth System Modeling, Atmos. Chem. Phys., 5, 433–444, 2005. 6855

Olson: World ecosystems (WE1.4): Digital ratser data on a 10 min geographic 1080 x 2160 grid square, edited by NOAA Natl. Geophsys. Data Cent. Boulder Colorado, global ecosystem database version 1.0: disc a edn., 1992. 6874

Pruppacher, H. and Klett, J.: Microphysics of Clouds and Precipitation, 2nd edition, Kluwer, Dordrecht, 954 pp., 1997. 6862

Slinn, S. and Slinn, W.: Predictions for Particle Deposition on Natural Waters, Atmos. Environ., 14, 1013–1016, 1980. 6863

Stier, P., Feichter, J., Kinne, S., Kloster, S., Vignati, E., Wilson, J., Ganzeveld, L., Tegen, I., Werner, M., Balkanski, Y., Schulz, M., and Boucher, O.: The Aerosol-Climate Model ECHAM5-HAM, Atmos. Chem. Phys., 5, 1125–1156, 2005.

Stull, R. B.: An Introduction to Boundary Layer Meteorology, Kluwer Academic Publishers, 1988. 6875, 6876

Wesely, M.: Parameterization of the surface resistances to gaseous dry depposition in regional-scale numerical models, Atmos. Environ., 23, 1293–1304, 1989. 6854, 6858, 6876, 6877, 6878, 6879, 6888

Wesely, M. and Hicks, B.: A review of the current status of knowledge on dry deposition, Atmos. Environ., 34, 2261–2282, 2000. 6854

Table 1. Assumed dimensionless reactivity coefficient (s_{reac}) and effective Henry coefficients (in mol/(dm^3 atm)) for the four gas phase species shown in the examples. Note: As the resistances for O_3 and SO_2 are pre-described following Wesely (1989) the Henry coefficients are the same as in Wesely (1989).

Species X	O_3	SO_2	HCOOH	PAN
$s_{reac}(X)$	1	0	0	0.1
$H(X)$	0.01	1×10^5	4×10^6	3.6

Table 2. Predefined gas phase tracer resistances (in s/m) in DRYDEP: R_{mes} is the mesophyll resistance, R_{cut} the cuticular resistance, $R_{s,soil}$, $R_{s,snow}$, $R_{s,ws}$ and $R_{s,wat}$ are the surface resistances for bare soil, snow/ice, wet skin and water, respectively. A, B and C indicate special cases as listed in Appendix A2.1.

Species	R_{mes}	R_{cut}	$R_{s,soil}$	$R_{s,snow}$	$R_{s,ws}$	$R_{s,wat}$
SO_2	1	10^5	C	B	100	1
O_3	1	10^5	400	2000	2000	2000
HNO_3	1	1	1	B	1	1
NO	A	10^5	10^5	10^5	10^5	10^5
NO_2	A	10^5	600	10^5	10^5	10^5

Table 3. pH classes according to Bates, 1995 and the respective soil resistances (in s/m) for SO_2.

pH class j	pH range	$R_{s,soil}(SO_2)$
1	pH≤5.5	115
2	5.5<pH≤ 7.3	65
3	7.3<pH≤8.5	25
4	8.5<pH	25
5	4<pH≤8.5	70

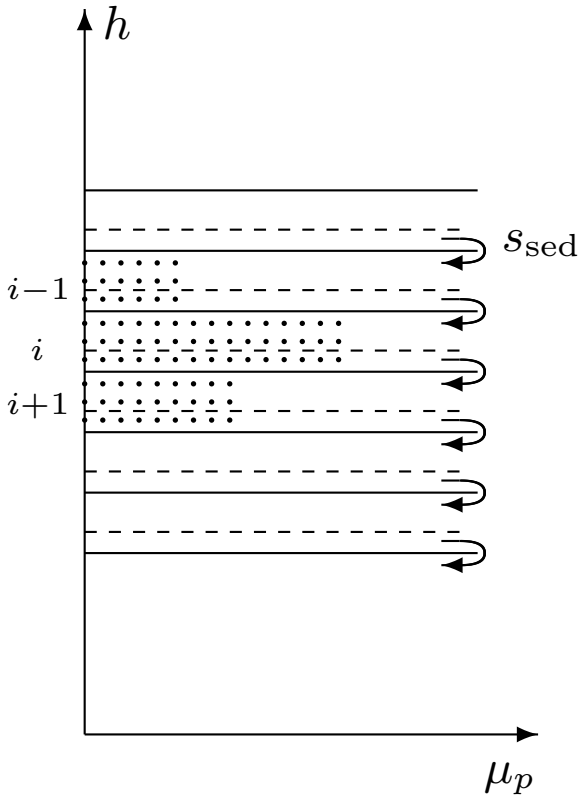

Fig. 1. Simple upwind scheme sedimentation assumes that if particles fall a distance s_{sed}, all particles from the lowermost layer of thickness s_{sed} of a grid box reach the next grid box below.

ACPD
6, 6853–6901, 2006

EGU

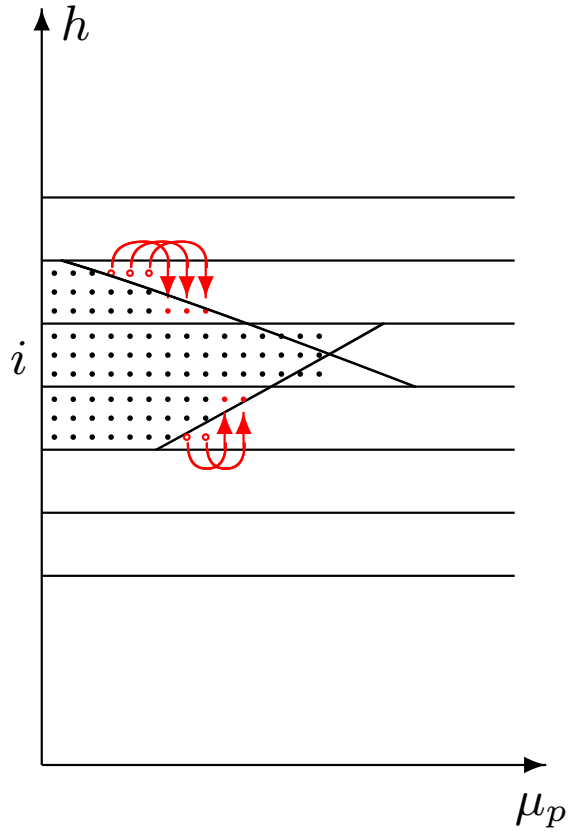

Fig. 2. In the trapezoid / first order scheme, the constant mixing ratios in each grid box (compare Fig. 1) are replaced by first order approximations.

ACPD
6, 6853–6901, 2006

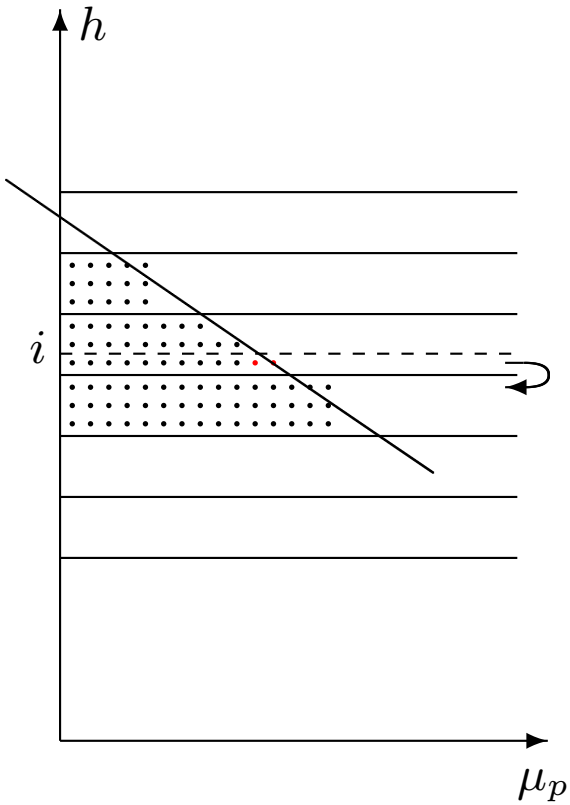

Fig. 3. The linear approximations above a local maximum lead to increased particle transport. The red circles indicate particles which do sediment in the trapezoid scheme but would not sediment in the simple upwind scheme.

ACPD
6, 6853–6901, 2006

EGU

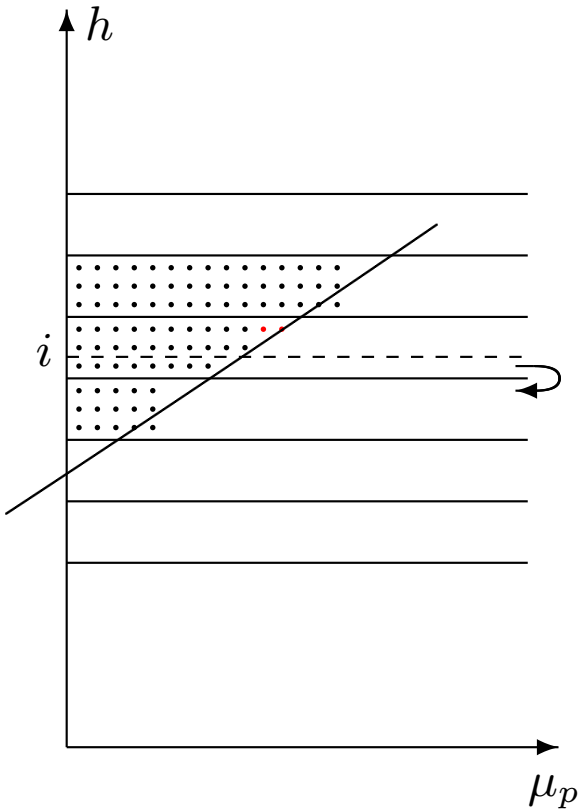

Fig. 4. Below a local maximum, linear approximations reduce the amount of transported particles. The red circles indicate particles which do not sediment in the trapezoid scheme but would sediment in the simple upwind scheme.

ACPD
6, 6853–6901, 2006

EGU

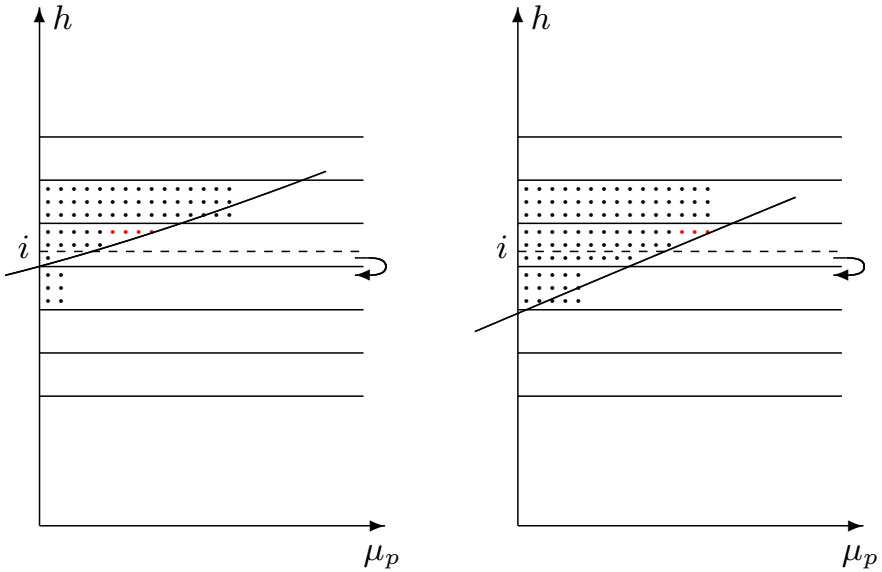

Fig. 5. The linear approximation below a local maximum is based on the mixing ratio μ_p from grid box i and $i-1$ above if $\mu_p(i)$ is relatively small compared to $\mu_p(i-1)$ (see left figure). If $\mu_p(i)$ is only slightly smaller than $\mu_p(i-1)$, the linear approximation is based on the μ_p values in grid boxes i and $i+1$ (see right figure). The criterion is which approximation yields the smaller trapezoid.

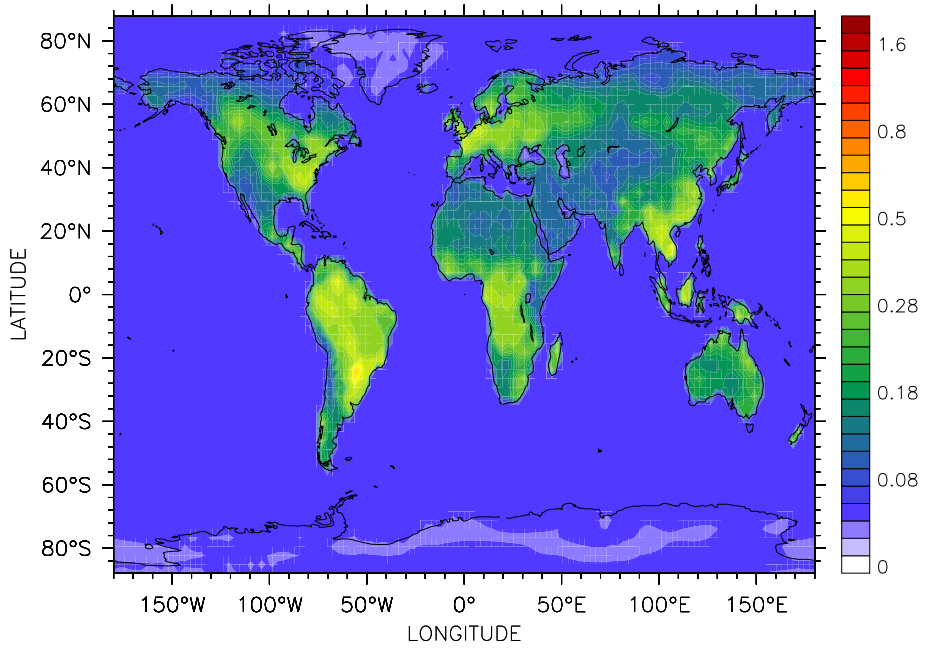

Fig. 6. Annually averaged dry deposition velocity of ozone (cm/s).

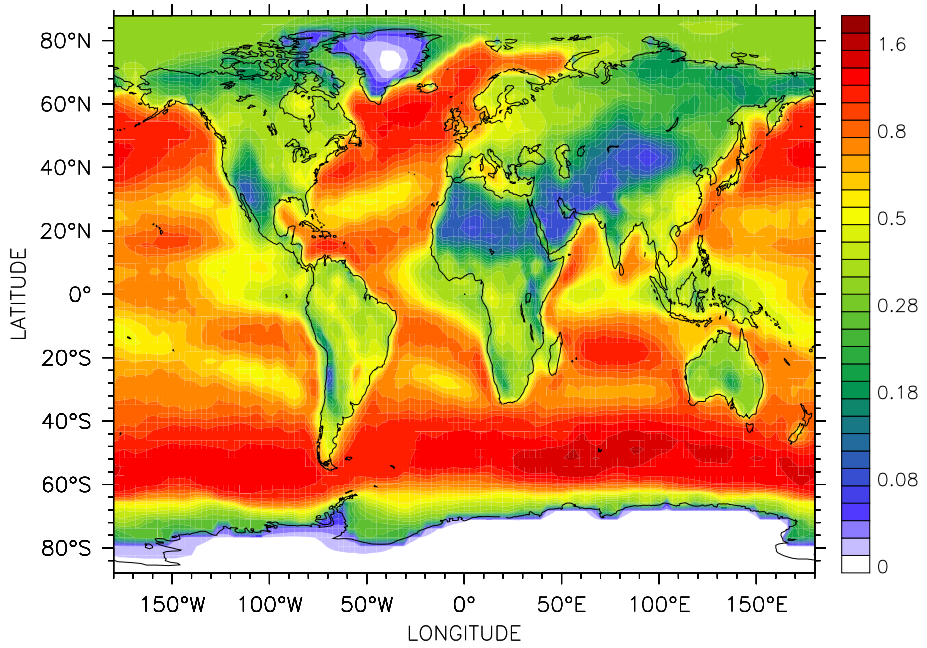

Fig. 7. Annually averaged dry deposition velocity of SO_2 (cm/s).

ACPD
6, 6853–6901, 2006

EGU

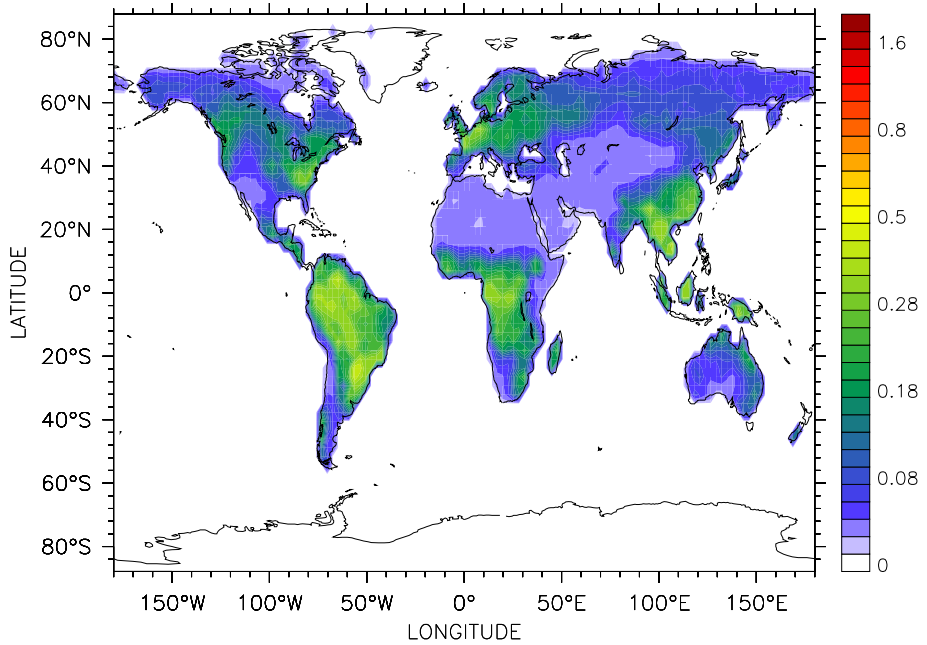

Fig. 8. Annually averaged dry deposition velocity of PAN (cm/s) as example of a relatively unsoluble, but reactive species.

ACPD
6, 6853–6901, 2006

EGU

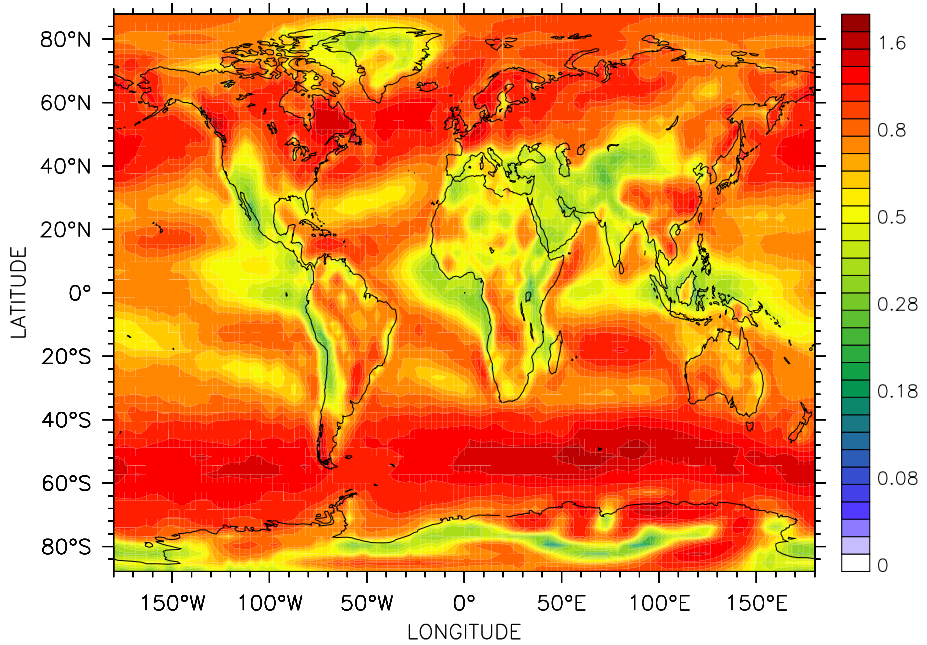

Fig. 9. Annually averaged dry deposition velocity of HCOOH (cm/s) as example of a soluble less reactive species.

ACPD
6, 6853–6901, 2006

EGU

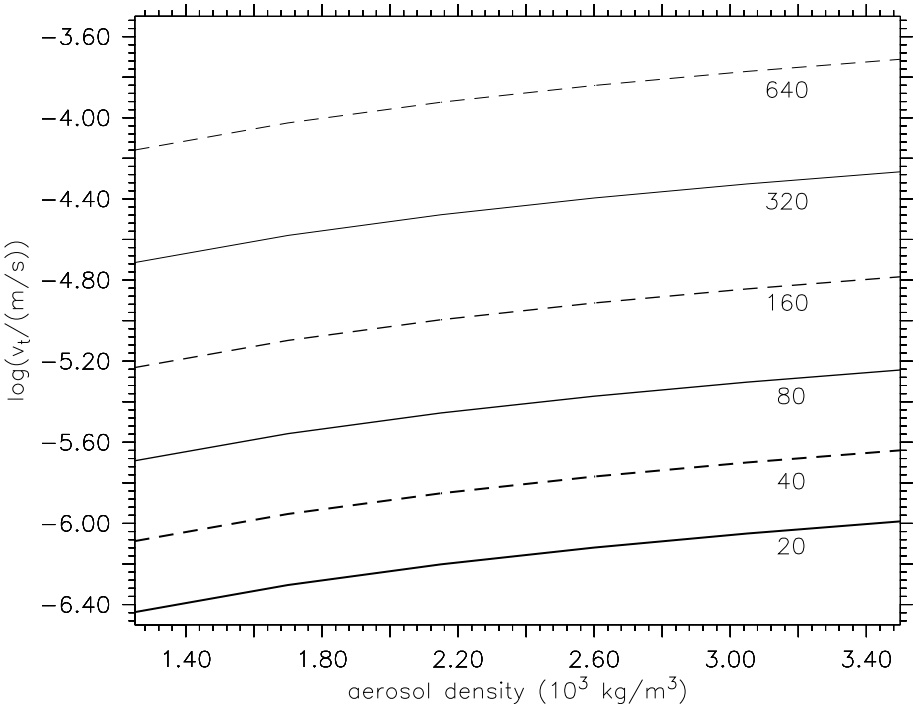

Fig. 10. Logarithm of the aerosol sedimentation velocities (in m/s) dependent on aerosol density (in kg/m^3). The velocities increase with increasing density and radius. The corresponding radii from bottom to top are 20 nm, 40 nm, 80 nm, 160 nm, 320 nm and 640 nm.

ACPD
6, 6853–6901, 2006

EGU

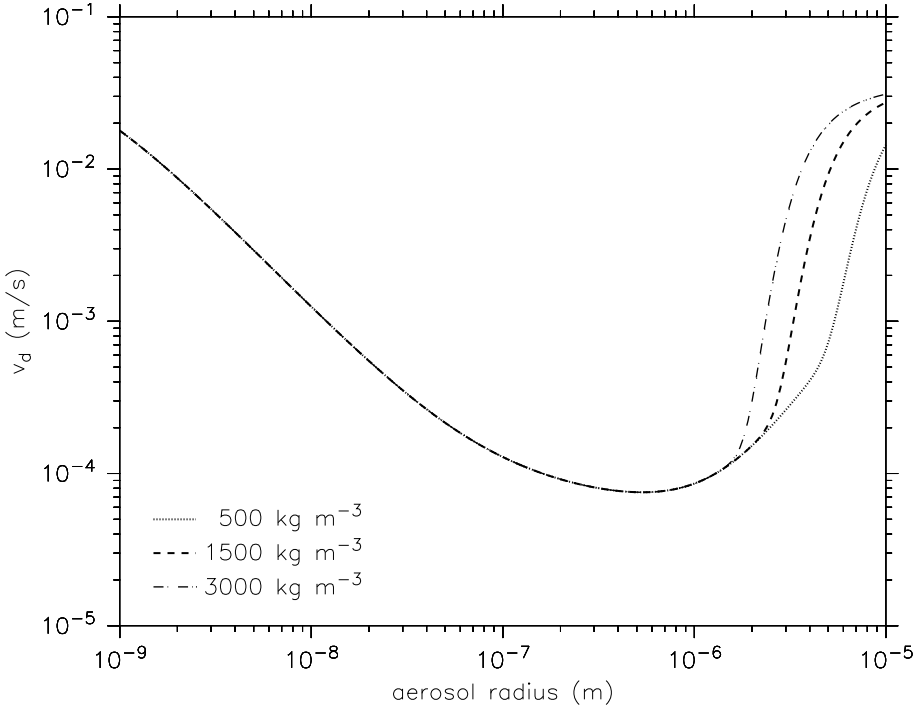

Fig. 11. Aerosol dry deposition (in m/s) dependent on the aerosol radius for three different aerosol densities.